Surface catalysis studied by in situ positron emission

TABLE 1 Results of model white-dwarf atmospheres for RE1629+781

Composition (He/H)	Temperature range (K) $V=13.0$	Temperature range (K) $V=13.75$	n_H Range (10^{19} cm^{-2}) $V=13.0$	n_H Range (10^{19} cm^{-2}) $V=13.75$
0	35,500–37,800	35,900–37,800	1.95–2.80	1.95–2.60
10^{-5}	36,400–37,600	36,400–37,300	1.70–2.30	1.80–2.30
3×10^{-5}	36,400–37,800	40,000	1.00–1.50	1.20
10^{-4}	No fit, therefore excluded.			
10^{-3}	No fit, therefore excluded.			

with the data (as in Fig. 3), and an allowed range of temperature and column density can be determined. Otherwise the model can be excluded. We have followed this procedure for compositions ranging from pure hydrogen to a He/H ratio of 10^{-3} using also the two extremes of V magnitude derived above to normalize the model spectra. The results are summarized in Table 1.

We conclude that the white dwarf has $35{,}500\ \mathrm{K} < T_{\mathrm{eff}} < 40{,}000\ \mathrm{K}$, which implies $M_V \approx 9.5$. The abundance of helium (by number) in the star's atmosphere is less than 10^{-4}. Our He/H ratio is similar to values determined by Exosat measurements[11] on DA white dwarfs with $T_{\mathrm{eff}} < 45{,}000$ K. We have assumed that the dM star makes negligible contribution to the EUV flux from the system. This is reasonable as the WFC count rate from the very active binary dMe flare star BY Dra (M.A.B., manuscript in preparation) placed at 43 pc, our closest estimate for RE1629+781, would be less than 1% of the total observed.

Although they have similar optical spectra, the Feige 24 DA+dM binary system and RE1629+781 show different characteristics in the EUV. Observations[12,13] of Feige 24 have shown a sharp fall-off of flux at the short-wavelength end of the EUV spectrum, but no evidence of the absorption edge at 228 Å that would result if helium was a principal source of opacity. The lack of strong absorption features in the EUV spectrum and the presence of narrow photospheric lines in the ultraviolet spectrum prompted Vennes *et al.*[13] to model the atmosphere of Feige 24 successfully as hydrogen-rich with small traces of 10 elements chosen to have photoionization edges in the soft X-ray and EUV bands. If such a source of opacity exists in RE1629+781, then the temperature would have to be significantly higher than we deduce from our models. Alternatively, and interestingly, the atmospheric compositions may be quite different. □

Received 21 June; accepted 8 October 1991.

1. Wells, A. *et al. Proc. SPIE* **1344,** 230 (1990).
2. Thorstensen, J. R., Charles, P. A., Margon, B. & Bowyer, S. *Astrophys. J.* **233,** 260–265 (1978).
3. Trümper, J. *Phys. Scripta* **T7,** 209 (1984).
4. Margon, B. *et al. Astrophys. J.* **209,** 525–535 (1976).
5. Liebert, J. & Margon, B. *Astrophys. J.* **216,** 18–22 (1977).
6. Margon, B. *et al. Astrophys. J.* **210,** L79–82 (1976).
7. Jacoby, G. H., Hunter, D. A. & Christian, C. A. *Astrophys. J. Suppl.* **56,** 257–281 (1984).
8. Straizys, V. & Kuriliene, G. *Astrophys. Space Sci.* **80,** 353–368 (1981).
9. Plummer, D., Schachter, J., Garcia, M. & Elvis, M. *The EINSTEIN Observatory IPC Slew Survey: FITS A3D/CD-ROM Version* (Smithsonian Astrophysical Observatory, 1991).
10. Barstow, M. A. *Mon. Not. R. astr. Soc.* **243,** 182–191 (1990).
11. Paerels, F. B. S. & Heise, J. *Astrophys. J.* **339,** 1000–1012 (1989).
12. Paerels, F. B. S., Bleeker, J. A. M. & Heise, J. *Astrophys. J.* **309,** L33–37 (1986).
13. Vennes, S., Chayer, P., Fontaine, G. & Wesemael, F. *Astrophys. J.* **336,** L25–28 (1989).
14. Bunclark, P. S. & Irwin, M. J. *Proc. Int. Colloq. on Statistical Methods in Astronomy, ESA Spec. Publ. no.* 201 (ed. Rolfe, E.) (European Space Agency, 1984).

Surface catalysis studied by *in situ* positron emission

G. Jonkers, K. A. Vonkeman, S. W. A. van der Wal & R. A. van Santen

Koninklijke/Shell-Laboratorium, Amsterdam, PO Box 3003, 1003 AA Amsterdam, The Netherlands

A COMPLETE understanding of heterogeneous catalytic processes requires quantitative *in situ* information on the concentrations of reactants present on the catalyst surface, but few techniques are available to supply this information. Here we show that positron-emitter labelling and scanning, using the isotopes ^{11}C, ^{13}N and ^{15}O, can be used to study the reactions taking place during the catalytic conversion of automotive exhaust. By introducing small pulses of labelled molecules into a reactant stream passing through the catalyst, *in situ* quantitative information on the concentrations and residence times of reactants in the reactor is obtained. The labels are detected using a positron camera, an imaging device adapted from nuclear medicine, and the recorded data are presented as 'reaction images', showing quantitatively the distribution of the label in the catalyst bed as a function of position and time. These data can then be used to quantify reaction kinetics by serving as the input to mathematical simulations based on elementary reaction steps.

Positron-emission computerized tomography (PET) is an imaging technique originating from nuclear medicine[1,2], where it is mainly applied as an *in vivo*, noninvasive medical research tool for the investigation of brain and heart diseases. PET has been applied industrially[3,4] by labelling the phase or particle of interest with a positron-emitting nuclide; examples are monitoring (nonreactive) flow of water in oil reservoir rock[3] and establishing flow profiles in extruders[4]. The availability of positron-emitting nuclides of carbon (^{11}C, half-life $t_{1/2}$ = 20.4 min), nitrogen (^{13}N, 9.96 min) and oxygen (^{15}O, 2.07 min) allows labelling of many reactant molecules. Because of these short half-lives, PET cameras are located near a radionuclide production facility, usually a cyclotron. Because of the high specific activity and the fact that individual molecules can be detected, experiments can be carried out using only minute amounts of labelled molecules (of the order of 0.1 pmol).

Because ^{11}C-, ^{13}N- or ^{15}O-labelled molecules are chemically indistinguishable from unlabelled ones, they offer the possibility of quantitatively measuring the presence and residence times of actual reactants on a catalyst surface under operating conditions (*in situ*). The ^{11}C-, ^{13}N- or ^{15}O-nucleus decays by emitting a positron, the antimatter counterpart of an electron. On an encounter between a positron and an electron, these two particles are instantaneously converted (annihilated) into two 511-keV γ-photons with high penetrating power, allowing noninvasive measurements. Simultaneous detection of both γ-photons by two individual detectors circuited in coincidence[2,5] defines the line on which the annihilation occurred (Fig. 1). The use of a PET camera as detection system should allow absolute positron-emitter concentrations to be monitored at a well-defined time and location, and thus allow 'imaging' of catalytic interactions. By using labelled molecules such as ^{11}CO, $C^{15}O$, ^{15}OO, $^{11}CO_2$, $C^{15}OO$ or ^{13}NN and a PET camera, we have demonstrated this technique in the investigation of automotive exhaust catalysis reactions.

A Pt-CeO_2/γ-Al_2O_3 exhaust catalyst was placed in a tubular plug-flow reactor (d = 7 mm) and continuously exposed to synthetic exhaust gas until steady-state conditions were obtained (Table 1). The conditions were chosen in such a way that the conversion of CO with O_2 into CO_2 was exclusively limited by intrinsic reaction kinetics and not by transport phenomena. The reactor was positioned horizontally in the centre of a NeuroECAT® PET instrument[6,7] (Fig. 1). A minute amount of ^{11}CO was added as a pulse to the synthetic exhaust gas passing through the reactor without disturbing the steady state of the catalyst (Table 1). The tomograph was operated in such a way that only events that were coincident at detectors in both opposing banks parallel to the flow tube were registered (Fig. 1). To obtain the optimal spatial resolution, we analysed the recorded

data by selecting either coincident events between directly opposite detectors (11 positions in total) or (average) coincidences between two opposite pairs of adjacent detectors viewing a single point on the reaction tube axis (10 positions). In this way the positron-emitter concentration at 21 equidistant (Δd = 1.1 cm)[6,7] positions over the reactor was measured simultaneously, and this measurement could be repeated every 1.2 s.

The recorded data, which have been corrected for radioactive decay, attenuation effects and detector efficiencies, are displayed in a 'reaction image' (Fig. 2) showing horizontally the axial concentration profile of the ^{11}C-label over the reactor. The vertical axis represents the time coordinate of the reaction image. The magnitude of the signal is represented in colours derived from a linearly scaled colour bar. As soon as the ^{11}CO pulse reaches the catalyst bed, it is adsorbed and can thereafter be converted into $^{11}CO_2$. The $^{11}CO_2$ is desorbed and carried away with the gas phase towards the outlet of the reactor. The $^{11}CO_2$ interacts with the ceria (CeO_2) on the catalyst surface through an adsorption/desorption process and is thereby delayed (see below).

The analysis of the recorded data is facilitated by drawing cross-sections through the images. This may be done either at a defined time, resulting in the ^{11}C-label distribution over the length of the reactor (at $t = 79$ s; PRF in Fig. 2), or at a defined position in the reactor, leading to the residence time distribution of the ^{11}C-label (at $x = -5.5$ cm; RTD in Fig. 2).

Under identical steady-state conditions (see Table 1) in separate experiments, six different labelled compounds were pulsed into the synthetic exhaust gas stream (Fig. 3*a*–*f*). Figure 3*a* demonstrates the plug-flow operation of the reactor when an inert gas ^{13}NN is led over an inert carrier (SiC). There is a considerable difference in residence time between the reaction images recorded for the $^{11}CO_2$ and C^{15}OO labelling experiments (Fig. 3*b* and *e* respectively) as well as between those for ^{11}CO and C^{15}O (Fig. 3*c* and *f*).

Comparison of reaction images 3*b* and *e* indicates that the C atoms of the CO_2 molecules entering the reactor have all left the catalyst bed before their original O atom partners arrive at the reactor outlet, demonstrating their separation during the reaction process. From these and other experiments[8], it was concluded that CO_2 molecules adsorb and decompose on the ceria surface. The ceria surface easily forms carbonate groups[9–11], and we therefore propose the formation of these species as an explanation. Under the reaction conditions, the cerium carbonate groups can decompose again to form CO_2 and ceria, where the O atoms of the desorbing CO_2 are not necessary identical to those of the originally adsorbed CO_2.

TABLE 1 Typical reaction and measuring conditions

Composition of synthetic exhaust gas	88.5 vol % Ar 10.0 vol % CO_2 1.0 vol % CO 0.5 vol % O_2
Flow rate	30 μmol s^{-1}
Catalyst system	3.9 g Pt-CeO_2/γ-Al_2O_3 (30–80 mesh)
Platinum loading	0.12 wt % Pt
Temperature	140 °C
Pressure	1 bar
Conversion	76 %
Injected pulse	
Total volume	200 μl (carrier added)
Cylindrical shape length	2 cm
Duration	0.4 s
Activity (^{11}C)	50 MBq (2 μCi)
Number of molecules (^{11}C)	0.15 pmol (carrier free)

The difference between the ^{11}CO and the C^{15}O labellin experiments (Fig. 3*c* and *f*) is due to the same effect. CO i oxidized on the platinum surface, and the CO_2 that is forme interacts with ceria. The bright narrow band at the bottom o the reaction image for ^{15}OO labelling experiments (Fig. 3*d*) i comparable to that of Fig. 3*a* and represents ^{15}OO molecule that do not interact with the catalyst bed. The remaining ^{15}O molecules adsorb and dissociate on the Pt surface, after whicl they react with adsorbed CO forming C^{15}OO. The C^{15}O desorbs from the Pt surface and becomes adsorbed on the ceri surface as described above. This causes the smeared activity distribution in the reaction image. The irreversible dissociativ nature of the O_2 adsorption is demonstrated by product iden tification of the ^{15}O-labelled species leaving the catalyst bed. Ir the initial peak, consisting of ^{15}O-labelled compounds tha passed through the catalyst bed without interaction, only ^{15}O molecules were present, whereas the remaining ^{15}O-atoms al left the catalyst bed in C^{15}OO molecules.

This positron-emitter labelling and scanning technique has been applied to an effectively one-dimensional (spatial) reactor. Here both the spatial (9 mm) and temporal (1.2 s) resolution achieved are dictated by the technical design of the NeuroECAT®, which was developed around 1980. Specially designed detector arrays may achieve a temporal resolution in the millisecond region. Future experiments may benefit from the progress made in the design of PET cameras, allowing monitoring of the three-dimensional distribution of ^{11}C-, ^{13}N- or ^{15}O-labelled molecules with a resolution close to its physical

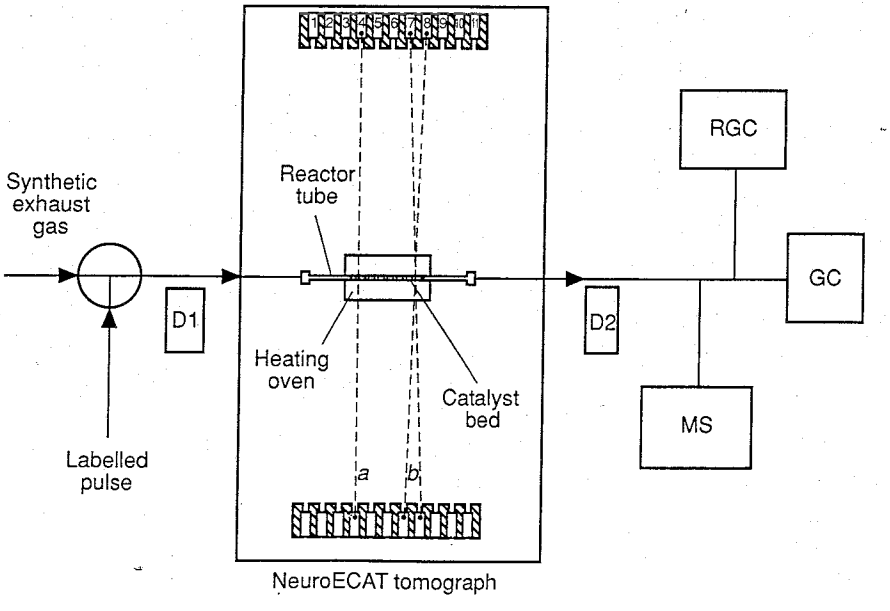

FIG. 1 Schematic drawing of the experimental set-up. D1 and D2 are separate radiation detectors for accurate monitoring of the inlet and outlet of the reactor system. The NeuroECAT® is a PET tomograph (technology from about 1980) with eight detector banks, each containing 11 individual detectors, arranged in an octagon. The detectors of the two banks parallel to the flow tube are drawn to scale. Dashed lines interconnect directly opposing (*a*) or opposing adjacent (*b*) detectors. Outlet gases from the reactor are analysed by a gas chromatograph (GC), a radio gas chromatograph (RGC) and a mass spectrometer (MS).

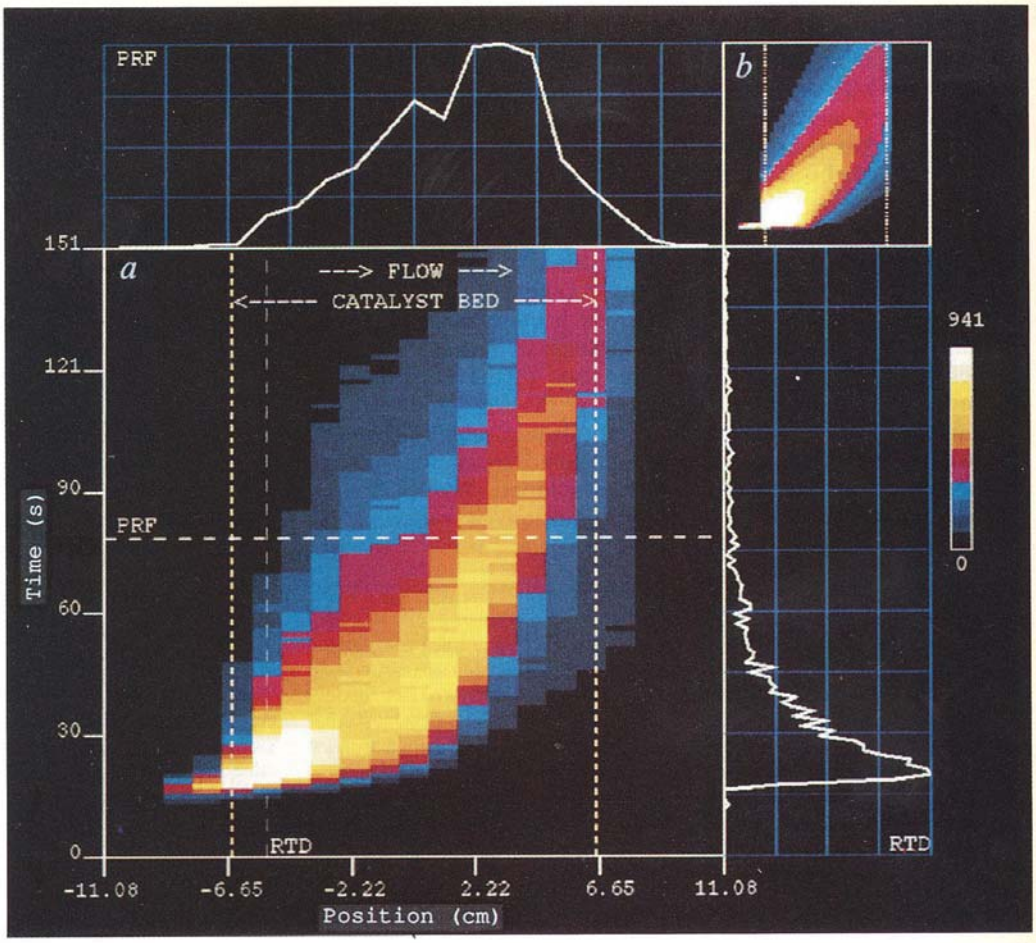

FIG. 2 *a*, Reaction image of a ^{11}CO experiment (see Table 1). The horizontal scale gives the position along the catalyst bed. The yellow dotted lines indicate the position of the catalyst bed. The vertical scale indicates the residence time. The colours indicate the ^{11}C-label concentration according to the linearly scaled colour bar. Also indicated are a profile (PRF) of the distribution of the label along the reactor axis (at time $t = 79$ s), and a residence time distribution (RTD) of the label (at position $x = -5.5$ cm). *b*, Computer simulation of the reaction image recorded for the ^{11}CO experiment.

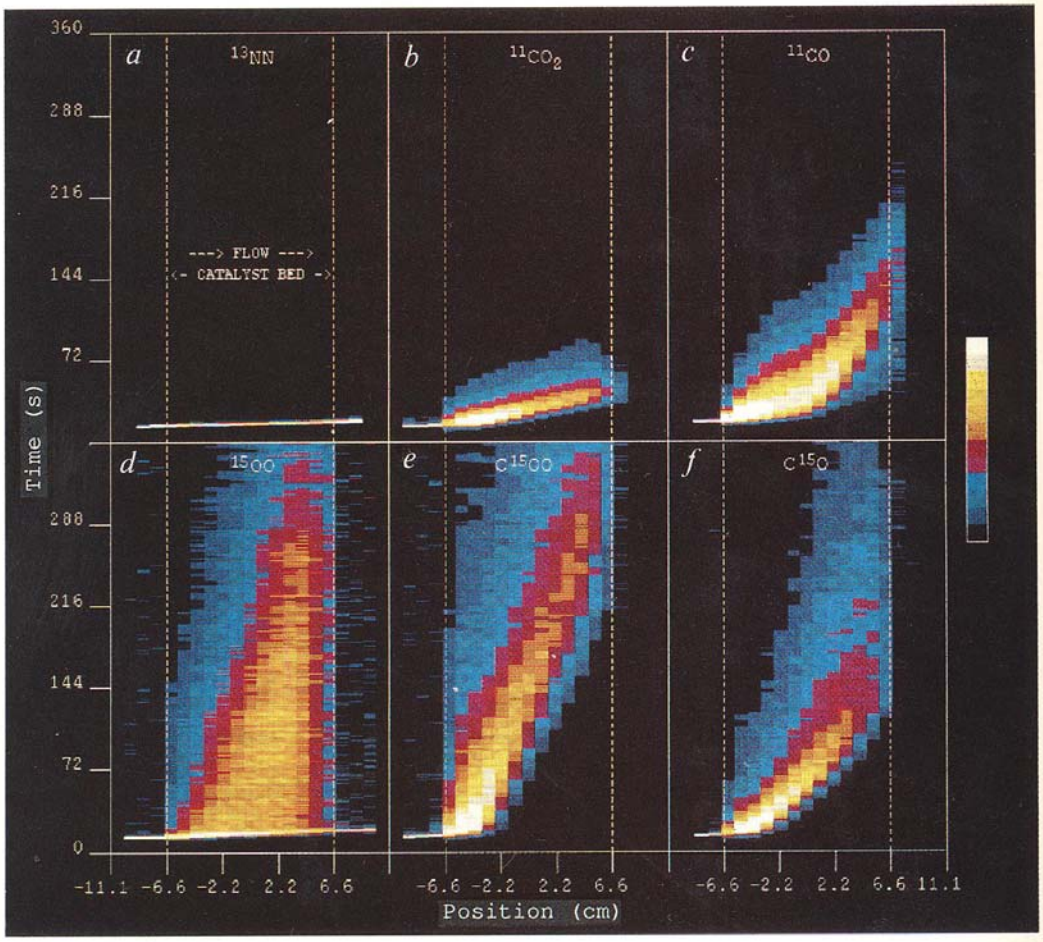

FIG. 3 Six reaction images of separate pulse experiments with different labels under identical conditions (see Table 1). *a*, ^{13}NN. The labelled molecules pass unhindered through the catalyst bed, showing their inertness. *b*, $^{11}CO_2$. The CO_2 molecules are delayed by the sorptive interaction with ceria on the catalyst surface. *c*, ^{11}CO. The delay of the CO molecules caused by adsorption on the Pt surface is followed by reaction to form CO_2, CO_2 desorption and the sorptive interaction between CO_2 and the ceria. *d*, ^{15}OO. Some of the labelled molecules pass unhindered through the catalyst bed (bright 'line' at bottom); the others are adsorbed on the platinum and react to form CO_2, which desorbs and becomes adsorbed on ceria with exchange of O atoms. This clearly shows the irreversible and dissociative nature of the oxygen adsorption on platinum. *e*, $C^{15}OO$. Interaction and O exchange between CO_2 and ceria. *f*, $C^{15}O$. CO oxidation on Pt, followed by CO_2 desorption and sorptive CO_2/ceria interaction with the O-atom exchange.

limit (2 mm)[1,2], ultimately dictated by the mean free path of the positron before annihilation.

The technique is not limited to automotive exhaust catalysis research. In homogeneous as well as in heterogeneous gas- or liquid-phase catalysis, both intrinsic kinetics and transport phenomena can be studied. The amount of data gathered in each experiment is very large and can therefore allow accurate quantification of reaction kinetics if used as the input to mathematical simulations rigorously based on elementary reaction steps. The simulation of the ^{11}CO pulse experiment (Fig. 2*b*) is the result of such a modelling study, which was based on kinetic constants for oxidation of CO obtained in surface science studies[8,12,13]. The labelled molecules used in the experiments are more or less directly available from the irradiated target. For this technique to be more widely applicable, labelling routes to basic reactants (for example, alkanes and aromatics for the petrochemical industry) have to be developed. Where *in situ* information from actual operating conditions is required, it should become a very useful technique. □

Received 15 July; accepted 14 October 1991.

1. *Positron Emission Tomography and Autoradiography—Principles and Applications for the Brain and Heart* (eds Phelps, M. E., Maziotta, J. C. & Schelbert, H. R.) (Raven, New York, 1986).
2. *The Physics of Medical Imaging* (ed. Webb, S.) (Adam Hilger, Bristol, 1988).
3. Van den Bergen, E. A., Jonkers, G., Strijckmans, K. & Goethals, P. *Int. J. Radiat. appl. Instrum. E: Nucl. Geophys.* **3**, 407–418 (1989).
4. Hawkesworth, M. R., Bemrose, C. R., Fowles, P. & O'Dwyer, M. A. in *Tomography and Scatter Imaging IOP Short Meetings Series* 19 (eds MacCuaig, N. & Holt, R.) 67–79 (Institute of Physics, Bristol, 1989).
5. Knoll, G. F. *Radiation Detection and Measurement* (Wiley, New York, 1989).
6. Williams, C. W. *et al. IEEE Trans. nucl. Sci.* NS-28, 1736–1740 (1981).
7. Hoffman, E. J., Phelps, M. E. & Huang, S. C. *J. nucl. Med.* **24**, 245–257 (1983).
8. Vonkeman, K. A. thesis, Technical Univ. Eindhoven (1990).
9. Jin, T., Okuhara, T., Mains, G. J. & White, J. M. *J. phys. Chem.* **91**, 3310–3315 (1987).
10. Daniel, D. W. *J. phys. Chem.* **92**, 3891–3899 (1988).
11. Li, C. *et al. J. chem. Soc. Faraday Trans. 1* **85**, 929–943 (1989).
12. Engel, T. & Ertl, G. in *Adv. Catal. 28* (eds Eley, D. D., Pines, H. & Weisz, P. B.) 2–78 (1979).
13. Lynch, D. T., Emig, G. & Wanke, S. E. *J. Catal.* **97**, 456–468 (1986).

ACKNOWLEDGEMENTS. We thank J. de Jong and H. Oosterbeek for their experimental assistance and K. Strijckmans, P. Goethals, I. Lemahieu and K. de Kesel, Institute for Nuclear Sciences, Rijksuniversiteit Ghent, Belgium for production of the radioisotopes, synthesis of the labelled reactants and help in experimenting with the NeuroECAT®.

Femtosecond laser control of a chemical reaction

E. D. Potter, J. L. Herek, S. Pedersen, Q. Liu & A. H. Zewail

Arthur Amos Noyes Laboratory of Chemical Physics, California Institute of Technology, Pasadena, California 91125, USA

THE critical stage in a chemical reaction—the progression through the transition state from reagents to products—occurs in less than a picosecond (10^{-12} s). Using laser pulses of femtosecond (10^{-15} s) duration it is possible to probe the nuclear motions throughout formation and break-up of the transition state[1,2]. The coherence and very short duration of these femtosecond pulses provides a means to influence the course of the reaction during this stage if the time resolution is made sufficiently short. Here we describe a demonstration of such control of a chemical reaction on the femtosecond timescale. Using two sequential coherent laser pulses, we can control the reaction of iodine molecules with xenon atoms to form the product XeI by exciting the reactants through the transition state, in a two-step process. The yield of product XeI is modulated as the delay between the pulses is varied, reflecting its dependence on the nuclear motions of the reactants.

For the most general elementary chemical reaction,

$$A+BC \rightarrow [A\cdot\cdot B\cdot\cdot C]^{\ddagger} \rightarrow AB+C$$

the products (AB + C) are formed from reagents (A + BC) after passing through the transition state $[A\cdot\cdot B\cdot\cdot C]^{\ddagger}$. This state, a 'collision complex', has six internal degrees of freedom, and energy can flow among them in a short time, typically picoseconds or less. At longer times, the distribution of energy becomes randomized and the system may reach a statistical limit in which the energy is shared among all degrees of freedom. If the energy is supplied to the reactants over a short timescale and further chemical change is induced after a prescribed time delay, it may be possible to control the trajectory of the nuclear motions towards product formation, either by the direct or the indirect formation of the transition state.

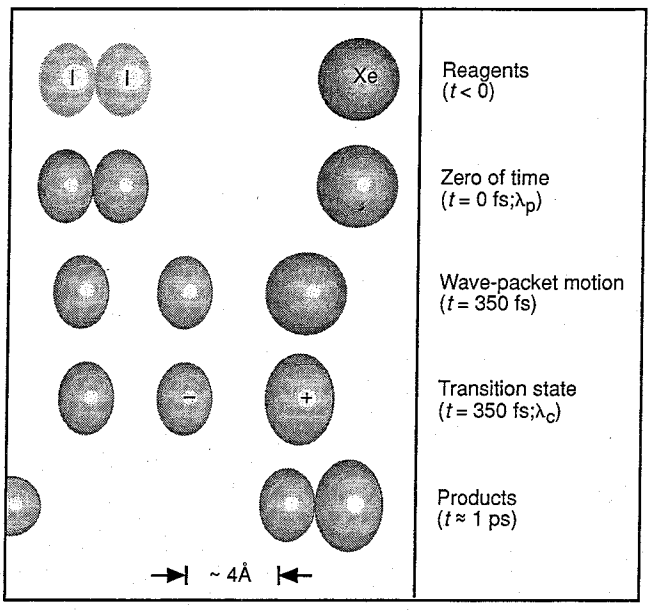

FIG. 1 Snapshots of the reaction A + BC → AB + C at different delay times. λ_p and λ_c refer to the pump and control wavelengths of the femtosecond pulses. The transition state for this case of $Xe+I_2$ is formed by electron harpooning from Xe to I_2. The dynamics of the reaction is complete in ~1 ps. The reaction is illustrated here for a particular internuclear configuration, without details of the pathway (see text), for simplicity.

Here we consider the bimolecular (atom-molecule) reaction of rare gas atoms (Xe) and halogen molecules (I_2). The reaction involves the translational motion of Xe towards I_2, the nuclear vibrational motion of iodine, and the formation of the transition state by Xe harpooning the I_2 through electron transfer:

$$Xe+I{-}I \rightarrow [Xe^{+}\cdot\cdot I^{-}\cdot\cdot I]^{\ddagger} \rightarrow XeI+I$$

The cross-section for this type of reaction is generally very large (~100–200 Å^2), and is essentially determined by the critical distance at which the harpooning occurs, which is typically larger than the van der Waals radius. Following the harpooning, the Coulomb interaction leads to the formation of XeI and the separation of product XeI from the iodine atom. This harpooning mechanism, introduced by Polanyi[3], is important for a variety of reactions in the gas phase, on surfaces and in the condensed phase[4–6]. For the rare gas/halogen systems, new studies have shown the importance of the harpooning mechanism in laser-assisted reactions (for reviews, see refs 7, 8).

The idea here is to exploit the nuclear motions (Fig. 1) on a femtosecond timescale. We use two femtosecond pulses separated by a time delay to pump and control the $Xe+I_2$ reaction. The first pulse, λ_p, creates a well defined, coherent wavefunction[9] (or more accurately, a wave packet) in an intermediate state, the B state of iodine. The wave packet moves[9] back and forth with a well defined period as the internuclear separation in the iodine molecule varies between 2.5 and 5 Å (Fig. 2). Some femtoseconds after the pump pulse, a second pulse λ_c is sent to lift this wave packet above the reaction threshold for reaction with Xe. Previous studies[10] have shown that this reaction involves the collision pair $I_2\cdot\cdot Xe$ (see below). If, for example, λ_c is